

Future Trends of Indoor SVOC Partitioning under Climate Change: Temperature-Dependent Partition Coefficients

Published as part of ACS ES&T Air special issue "Indoor Chemistry in the Context of a Changing Climate".

Jiangyue Zhao, Tunga Salthammer, Erik Uhde, Lukas Wittmann, and Alexandra Schieweck*



Cite This: ACS EST Air 2026, 3, 780–793



Read Online

ACCESS |

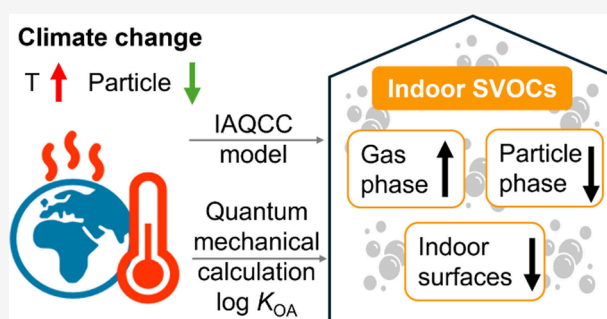
Metrics & More

Article Recommendations

Supporting Information

ABSTRACT: We used ten representative semivolatile organic compounds (SVOCs) to investigate how changes in temperature and particle concentration affect future concentrations and partitioning of SVOCs in the gas phase, particulate phase, and on surfaces in the indoor environment. Using quantum mechanical methods and quantitative structure–activity-relationship (QSAR) tools, accurate temperature-dependent octanol/air partition coefficients (K_{OA}) and vapor pressures (P_L) of the subcooled liquid were calculated. Under the pessimistic greenhouse gas emissions scenario SSP5–8.5 as projected by the Intergovernmental Panel on Climate Change (IPCC), an annual shift in the SVOC equilibrium concentration between gas phase, particle phase, and surface by up to 30% is expected until 2100. The SSP5–8.5 scenario leads to higher SVOC emission rates and changes in the organic film thickness on surfaces. However, since primarily annual averages are considered, these temperature-related changes are small. Nevertheless, a model calculation for the emission rate of DINCH, taking into account extreme daily indoor temperatures, was performed. Since many developments up to 2100 can only be estimated, simplifying assumptions were made for emission rates, film thickness, and other parameters.

KEYWORDS: Shared Socio-economic Pathway (SSP), temperature-dependent octanol/air partition coefficients (K_{OA}), gas/particle partitioning, sorption to surfaces, quantum-mechanical calculation, quantitative structure–activity-relationships (QSAR)



1. INTRODUCTION

Global warming is progressing faster than ever before in human history. According to the Copernicus Climate Change Service, the global average temperature in 2024 already exceeded the limit of 1.5 °C above preindustrial levels set in the Paris Climate Agreement.¹ The outdoor climate has a direct influence on the indoor climate through solar radiation and the air mass exchange via the building envelope, including heat, humidity, air pollutants, etc. Rising ambient temperatures, shifting humidity, and increasingly frequent extreme weather events not only impact thermal comfort but also alter the emission, reaction, partitioning, and dynamics of indoor gas and particle pollutants.^{2,3} These processes subsequently impact indoor air quality, affecting human health and well-being.

Among these pollutants, semivolatile organic compounds (SVOCs) have drawn particular attention due to their long-term persistence in dwellings and thus prolonged exposure times of the residents. Epidemiological and toxicological studies link exposure to certain types of SVOCs with endocrine disruption, respiratory effects, carcinogenicity, and other health risks.^{4–8} The list of the most frequently detected substances

includes phthalates, flame retardants, UV filters, synthetic musk compounds, as well as perfluoroalkyl and polyfluoroalkyl substances (PFAS).^{9–12}

SVOCs in indoor environments involve complex dynamic processes and partitioning mechanisms (see Figure 1). SVOCs have been widely detected in indoor air, settled dust, and on material surfaces.^{13–21} The indoor primary sources including building and decorative materials, paints, textiles, electronics, cosmetics, and consumer goods.²² Due to the slow release of SVOCs from sources and their tendency to sorb on surfaces, they can persist for a long time once introduced to indoor spaces.²³ SVOCs in the air are also exchanged between indoor and outdoor spaces through ventilation and penetration via building cracks. This dynamic process can lead to redistribution of indoor SVOCs in air and on surfaces. Reducing the air

Received: October 7, 2025
Revised: February 11, 2026
Accepted: February 12, 2026
Published: February 27, 2026



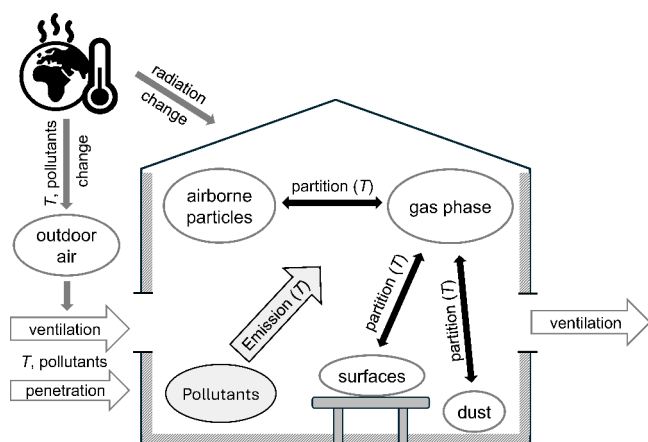


Figure 1. Partitioning of released and infiltrated chemical pollutants between different compartments in the indoor environment. The temperature-dependent processes considered in this work are marked with (T).

concentration through air exchange or other measures will in turn increase the emission rate from the source materials until the system reaches a new equilibrium.^{24,25}

Various model approaches have been developed to describe these key processes and predict the partitioning of indoor SVOCs between different indoor compartments, mostly under equilibrium conditions. As far as surfaces are concerned, the concentration of airborne particles significantly influences the SVOC flux in the boundary layer.²⁶ Based on a mass transfer model for SVOC emissions from building materials,²⁷ Xu and Little²⁸ found that higher concentrations of airborne particles can lead to higher SVOC emission rates from materials. Later this work was extended by considering interactions with indoor surfaces,²⁶ dust, and human skin.²⁹ Junge³⁰ and Pankow³¹ developed the first models for describing the partitioning between gas phase and particle phase using a gas/particle partition coefficient (K_p). K_p can be estimated either from the vapor pressure³¹ or from the octanol/air partition coefficient (K_{OA}).³² Based on these and other studies, Weschler and Nazaroff²³ provide a framework to understand and characterize the equilibrium partitioning of SVOCs in the gas phase with airborne particles, settled dust, indoor surfaces and human skin.

Indoor environmental parameters such as temperature and airborne particle concentration have strong influence on mass transfer (emission/sorption of indoor materials) and partitioning processes of indoor SVOCs. Previous experimental studies have shown that higher temperatures lead to higher emission rates and gas phase concentrations of SVOCs.^{33–35} Zhou et al.³⁶ found that temperature has a strong negative influence on K_p . Based on the Clausius–Clapeyron equation and Pankow’s description of the absorptive SVOC gas/particle mechanism,³⁷ Wei et al.³⁸ developed a theoretical relationship between K_p and temperature. Salthammer and Goss³⁹ used a poly parameter linear free energy relationship (pp-LFER) approach to predict temperature-dependent K_p values.^{40,23,26}

The crucial parameters for determining reasonable K_p values are K_{OA} and the vapor pressure (P_L) of the subcooled liquid. However, these are subject to large uncertainties for many SVOCs and are often only known for 298 K.^{40,41} Therefore, for the calculations required in this work, great emphasis was placed on determining the temperature-dependent K_{OA} and P_L of the nine target SVOCs using quantum mechanical methods. Based on a critical comparison with literature data, we conclude that the values finally used represent the best possible predictions. Di-*n*-butyl phthalate (DnBP) serves as the reference, as reliable data are available for this compound.

Climate change is expected to alter indoor climate and pollutant levels, and based on the literature data mentioned above, these changes will consequently affect the partitioning of SVOCs indoors. However, the extent to which these changes will influence future indoor SVOC levels remains unclear. To address this gap, the present study takes into account the expected changes caused by climate change and predicts future indoor SVOC concentrations, as well as their partitioning between the gas phase, the particle phase, and indoor surfaces. Due to the uncertainty of forecasts and climate models, our calculations include several simplifying assumptions. As previously stated,⁴² the results should therefore be interpreted as reasonable trends.

2. MATERIALS AND METHODS

2.1. Indoor Air Simulation Model and Selected SVOCs

The Indoor Air Quality and Climate Change (IAQCC) model⁴³ serves to calculate long-term developments of indoor climate, as well as gas and particle concentrations. IAQCC is a holistic approach that builds on existing models. The different modules consider building

Table 1. Selected SVOCs and Their Properties

SVOC category	Compound	Abbreviation	CAS-No.	Mol. formula	MW ^c (g mol ⁻¹)
UV Stabilizers	Benzophenone-12	BP-12 ^b	1843–05–6	C ₂₁ H ₂₆ O ₃	326.4
	Benzophenone-3	BP-3	131–57–7	C ₁₄ H ₁₂ O ₃	228.2
	2-(2 <i>H</i> -benzotriazol-2-yl)-4,6-di- <i>tert</i> -pentylphenol	UV-328	25973–55–1	C ₂₂ H ₂₉ N ₃ O	351.5
Plasticizers	Diisononyl cyclohexane-1,2-dicarboxylate ^a	DINCH	166412–78–8	C ₂₆ H ₄₈ O ₄	424.7
	Di- <i>n</i> -butyl phthalate	DnBP	84–74–2	C ₁₆ H ₂₂ O ₄	278.3
	2,2,4-Trimethyl-1,3-pentanediol diisobutyrate	TXIB	6846–50–0	C ₁₂ H ₂₄ O ₃	286.4
Musk compounds	Galaxolide	HHCB	1222–05–5	C ₁₈ H ₂₆ O	258.4
Per- and Polyfluoroalkyl Substances (PFAS)	Perfluorooctanoic acid	PFOA	335–67–1	C ₈ HF ₁₅ O ₂	414.1
Organophosphate Flame Retardants (OPFR)	Tris-chloropropyl phosphate	TCPP	13674–84–5	C ₉ H ₁₈ Cl ₃ O ₄ P	327.6
	Triphenyl phosphate	TPP	115–86–6	C ₁₈ H ₁₅ O ₄ P	326.3

^aMixture of isomers. Calculations refer to bis(7-methyloctyl) 1,2-cyclohexanedicarboxylate. ^bOther name: UV-531. ^cData from PubChem (<https://pubchem.ncbi.nlm.nih.gov/>).

physics, indoor pollutant emissions, gas phase chemical reactions and particle dynamics, mold growth on indoor surfaces, as well as the assessment of indoor thermal comfort and risk of exposure to indoor air pollutants. In particular, the building physics simulation is based on the WUFI@Plus software (Wärme Und Feuchte Instationär, engl. heat and moisture transiency). The indoor chemistry simulation was developed based on the well-established comprehensive Master Chemical Mechanism (MCM, v3.3.1),^{44,45} and the simulation of indoor particle dynamics was developed based on the Indoor Aerosol Model (IAM).^{46–48} Details about the model and the implemented modules have been published previously.^{43,44}

The IAQCC model considers key processes and parameters for simulating gas and particle reactions and dynamics in indoor spaces. Changes in the concentrations of gas phase and particle phase pollutants indoors are determined by indoor/outdoor air exchange (ventilation and infiltration), emissions from occupants' activities, furniture or building materials, resuspension of coarse particles, coagulation of submicrometer particles, and losses/gains due to gas-phase reactions. The general balance equation is mathematically described by eq 1,

$$\frac{dC_{in}}{dt} = P \cdot \lambda \cdot C_{out} - \lambda \cdot C_{in} - \lambda_d \cdot C_{in} + \sum_{i=1}^n \frac{E_i}{V} + \sum_{j=1}^n \frac{R_j}{V} \pm J_{Coag} \pm \xi \cdot \psi_{gas} \quad (1)$$

where C_{in} and C_{out} are the indoor and outdoor gas/particle concentrations ($\# \text{ cm}^{-3}$ or $\mu\text{g m}^{-3}$). P is the outdoor air penetration factor. λ is the air change rate (h^{-1}), and λ_d is the deposition rate on indoor surfaces (h^{-1}). E_i is the emission rate of source i ($\# \text{ h}^{-1}$ or $\mu\text{g h}^{-1}$), and V is the room volume (m^3). R_j is the resuspension rate of source j for coarse particles ($\# \text{ h}^{-1}$ or $\mu\text{g h}^{-1}$). J_{Coag} is the coagulation rate of particles. ψ_{gas} is the reaction rate due to gas-phase reactions, and the ξ represents the yield of secondary organic aerosols (SOA).

This work focuses on SVOCs that might be of concern in the future. The selected chemicals cover a wide range of application categories as well as physical and chemical properties and are listed in Table 1. SVOCs that have been extensively studied in the past, such as the plasticizers di(2-ethylhexyl) phthalate (DEHP) and benzyl *n*-butyl phthalate (BnBP), were not taken into account as many of them already have been banned in various countries for decades^{49,50} and are expected to be phased out gradually. Nevertheless, di-*n*-butyl phthalate (DnBP) was included in the calculations, as valid experimental and predicted data are available for this substance, which allows for a better assessment of the reliability of the prediction tools.

2.2. The Temperature Dependence of Partition Coefficients

To better predict the effects of climate change, data on key parameters for estimating SVOC partitioning at different temperatures are crucial.

When two solvents α and β are brought into contact with each other at a certain temperature, an equilibrium is established which depends on the miscibility of these phases at that temperature. If there is no or only low mutual solubility of the two solvents, two phases are formed, between which a solute i is partitioned. The equilibrium depends on the chemical potentials with $\mu_{i,\alpha} = \mu_{i,\beta}$, i.e. the sum of the intramolecular and intermolecular energies in each phase. These, in turn, are a function of pressure, temperature, and the chemical composition of that phase.⁵¹

In an ideal system, the partitioning of i between α and β is a direct function of the mole fractions $x_{i,\alpha}$ and $x_{i,\beta}$. In a nonideal system, the activity a_i in each phase must be considered with $a_i = \gamma_i \cdot x_i$, where γ_i is the activity coefficient.⁵² In the nonequilibrium state, the difference in chemical potentials (see eq 2) corresponds to the free energy $\Delta_{\alpha\beta}G_i$, resulting in a phase transfer of i between α and β until equilibrium is reached.

$$\mu_{i,\alpha} - \mu_{i,\beta} = RT \ln \frac{x_{i,\alpha}}{x_{i,\beta}} + RT \ln \frac{\gamma_{i,\alpha}}{\gamma_{i,\beta}} \quad (2)$$

Equation 3 is then obtained for the partition coefficient $K_{i,\alpha\beta}$ with $\mu_{i,\alpha} - \mu_{i,\beta} = 0$.

$$\ln K_{i,\alpha\beta} = \ln \frac{x_{i,\alpha}}{x_{i,\beta}} = - \frac{RT \ln \gamma_{i,\alpha} - RT \ln \gamma_{i,\beta}}{RT} = - \frac{\Delta_{\alpha\beta}G_i}{RT} \quad (3)$$

Enthalpy $\Delta_{\alpha\beta}H_i$ and entropy $\Delta_{\alpha\beta}S_i$ of phase transfer are related to the free energy $\Delta_{\alpha\beta}G_i$ via the Gibbs equation $\Delta_{\alpha\beta}G_i = \Delta_{\alpha\beta}H_i - T \cdot \Delta_{\alpha\beta}S_i$. Due to the small difference between two temperatures T_1 and T_2 in the considered range of 283 to 323 K, it can be approximately assumed, that $\Delta_{\alpha\beta}H_i$ and $\Delta_{\alpha\beta}S_i$ are independent of temperature. This yields the van't Hoff equation 4 in its differentiated form and equation 5 in its integrated form.⁵¹

$$\frac{d(\ln K_{i,\alpha\beta})}{dT} = \frac{\Delta_{\alpha\beta}H_i}{RT^2} \quad (4)$$

$$\ln \frac{K_{i,\alpha\beta}(T_2)}{K_{i,\alpha\beta}(T_1)} = - \frac{\Delta_{\alpha\beta}H_i}{R} \left[\frac{1}{T_2} - \frac{1}{T_1} \right] \quad (5)$$

These considerations also apply to the equilibrium of a component i between its liquid phase and its vapor phase, resulting in the Clausius–Clapeyron equation analogous to the van't Hoff equation 5 with the enthalpy of vaporization $\Delta_{\text{vap}}H_i = \Delta_{\alpha\beta}H_i$.

Using quantum mechanical methods, partition coefficients and the vapor pressure P_i of the subcooled liquid can be directly determined from $\Delta_{\alpha\beta}G_i$ for the desired temperature. The workflow applied here includes the calculation of extensive conformer ensembles with semiempirical methods and refinement through density functional theory, taking into account solvation models, especially COSMO-RS, and thermostatical contributions.^{40,41}

2.2.1. Temperature Dependence of the Octanol/Air Partition Coefficient. The standard temperature for the experimental determination or prediction of the octanol/air partition coefficient (K_{OA}) is 298 K. For conversion to other temperatures, the internal energy of phase transfer $\Delta_{OA}U_i$ or the enthalpy of solvation $\Delta_{OA}H_i$ is required, where both quantities are related via equation 6.

$$\Delta_{OA}U_i = \Delta_{OA}H_i + RT \quad (6)$$

Due to the high laboratory effort, $\Delta_{OA}U_i$ and $\Delta_{OA}H_i$ are only rarely measured.⁵³ A good alternative are prediction tools, for which several reliable approaches exist. The method of Mintz et al.⁵⁴ is based on the poly parameter linear free energy relationship (pp-LFER) given by equation 7 using the Abraham descriptors V_i (McGowan molar volume), L_i (logarithm of the hexadecane/air partition coefficient), S_i (polarizability/dipolarity), A_i (solute hydrogen bond acidity), and B_i (solute hydrogen bond basicity).

$$\Delta_{OA}H_i = 1.6 \cdot V_i - 9.7 \cdot L_i + 6.0 \cdot S_i - 53.7 \cdot A_i - 9.2 \cdot B_i - 6.7 \quad (7)$$

Baskaran et al.⁵⁵ developed a set of relationships for the prediction of $\Delta_{OA}U_i$ (kJ mol^{-1}). We chose equation 8, which does not require pp-LFER parameters, since experimental Abraham descriptors are not available for all of the compounds discussed.

$$\Delta_{OA}U_i = -8.75 \cdot \log K_{OA} - 5.07 \quad (8)$$

For the SVOCs selected in this study, experimentally determined Abraham descriptors for pp-LFER calculations were taken from the database of Ulrich et al.⁵⁶ when available. For the other substances, the descriptors were calculated from the SMILES structures (see Table S1 in the Supporting Information). Okeme et al.⁵⁷ provide experimental $\Delta_{OA}U_i$ values at 298 K for BP-3, HHCb, TCPP, and TPP. The internal energies of phase transfer $\Delta_{OA}U$ were calculated according to the methods of Mintz et al.⁵⁴ (eq 7) and Baskaran et al.⁵⁵ (eq 8). All values are summarized in Table S2 in the Supporting Information.

By inserting $\Delta_{OA}U_i$ into equation 5 and converting to the decimal logarithm, equation 9 is obtained.

$$\log K_{i,OA}(T_2) = \log K_{i,OA}(T_1) - \frac{\Delta_{OA}U_i}{R} \left[\frac{1}{T_2} - \frac{1}{T_1} \right] \cdot \log e \quad (9)$$

The calculation methods for the temperature dependence of the vapor pressure P_L of the subcooled liquid were also discussed and can be found in Section S1.1 of the Supporting Information.

2.2.2. Quantum-Mechanically Generated $\log K_{OA}$ Data.

Accurate quantum-mechanical calculations of thermodynamic properties, such as partition coefficients and vapor pressures, require extensive sampling of each molecule's conformational space.⁵⁹ Since every unique structure contributes differently to the Boltzmann-weighted free energy, omitting important minima can introduce significant errors in the computed values. For this, we employ the GOAT conformer-sampling tool⁶⁰ in conjunction with the GFN2-xTB tight-binding method⁶¹ and the ALPB solvation model.⁶² The obtained ensemble was subsequently optimized using the r²SCAN-3c composite method,⁶³ combined with the CPCM solvation model.⁶⁴ This step was performed individually for each substance-solvent combination. Finally, higher-level electronic energies are used in combination with the COSMO-RS⁶⁵ solvation model to obtain the partition coefficients and vapor pressures of the subcooled liquid.

Quantum chemical calculations were performed with xTB 6.7.0⁶⁶ and ORCA 6.0.1.⁶⁷ The workflows utilized GOAT⁶⁰ and CENSO 2.0.⁶³ The conformational sampling and subsequent optimization was done using GFN2-xTB⁶¹ with the ALPB solvation model and the r²SCAN-3c composite method⁶³ with the CPCM solvation model. Subsequent higher-level range-separated hybrid calculations utilize ω r²SCAN-D4/def2-TZVPPD.⁶⁸ Matching general-purpose auxiliary basis sets are constructed on the fly⁶⁹ and the RIJCOSX⁷⁰ approximation was used for all hybrid calculations. COSMO-RS is calculated using TurboMole 7.9.0⁷¹ with COSMOtherm C30–1601 and uses per default BP86/def-TZVP level of theory.⁷²

2.3. IAQCC Model: Test House Settings

In this work, we simulated the dynamics of selected SVOCs for expected long-term and short-term future climate scenarios under the conditions of a single-family test house, which is located in the rural area of Leipzig, Germany (latN: 51°22', longE: 12°30'). The solidly constructed house was built in 1995 with renewed double-glazed windows. It is naturally ventilated with a mean ventilation rate of $\lambda = 0.5 \text{ h}^{-1}$. The calculations were performed for a living room with the dimensions of $4 \times 4.5 \times 2.55 \text{ m}^3$.

Initial weather data were taken from nearby government measurement stations published by Deutscher Wetterdienst (DWD; reference coordinates 51,3731° N, 12,5063° O, access date 26.07.2024). Initial outdoor concentrations of ozone, PM_{2.5} and PM₁₀ were taken from historical data measured in Germany (average of all stations with available data) from the database published by the European Environment Agency.⁷³ Details of the initial data can be found in the publication by Zhao et al.⁴²

The sixth assessment report of the Intergovernmental Panel on Climate Change (IPCC) addresses climate responses in five illustrative scenarios, known as Shared Socio-economic Pathways (SSP), which cover a range of possible future developments in greenhouse gases (GHG), land use, and air pollutants.⁷⁴ In our previous work by Zhao et al.,⁴² simulation results of indoor climate and particle concentrations of PM_{2.5} and PM₁₀ in this test house were validated. Furthermore, in this earlier study⁴² we also made a long-term prediction of indoor particle concentrations under selected IPCC scenarios. The reactions and dynamics of a typical indoor reaction system were simulated using the limonene/ozone/OH reaction as example. These results allowed the SOA produced by this reaction to be included in the simulation of indoor particle concentrations. The input parameters for the test house are summarized in Table S3 of the Supporting Information, including parameters for building physics and air pollutant simulations.

In the current work, calculated indoor SVOC concentrations and partitioning were based on simulated indoor climate and particle concentrations in the test house. Two SSP scenarios were selected: SSP1–2.6 and SSP5–8.5, covering the low and high levels of GHG

emissions, respectively. IPCC projections^{75,76} of annual mean changes in future outdoor temperatures, concentrations of ozone and PM_{2.5} are summarized in Table S4 of the Supporting Information. Since the prediction for PM₁₀ was not available, for simplicity it was assumed that PM₁₀ follows the same trend as PM_{2.5}, using the same change factor.

2.4. Simulation of SVOC Dynamics Indoors

2.4.1. SVOC Concentrations in Indoor Air. Our simulations take into account both SVOC indoor emission sources and losses from indoor-outdoor air exchange. Only limited data is available in the literature regarding indoor concentration levels of the target SVOCs. The relevant references are summarized in Table 2 and Table

Table 2. Mean Value of Literature Data on the Indoor Air Concentration, Simulated Indoor Air Concentrations, and Emission Rates in the Test House for Seven Target SVOCs under Current Climate (by 2020)^b

Compound	Mean concentration of literature values (ng m ⁻³) ^a	Simulated concentration (gas + particle phase, ng m ⁻³)	Simulated emission rate (ng h ⁻¹)
BP-3	2.9 ²⁰	3.0	71
DINCH	61 ^{77,78}	64	1.5 × 10 ³
HHCB	97 ^{16,79}	103	2.4 × 10 ³
PFOA	0.1 ^{80,81}	0.1	2
TCPP	208 ^{19,79,82}	213	5.0 × 10 ³
TPP	3.5 ^{79,82}	3.5	84
TXIB	1.4 × 10 ³⁸³	1.5 × 10 ³	3.4 × 10 ⁴

^aSee Table S5 in the Supporting Information for details of the literature study. ^bNo data are available for BP-12 and UV-328.

S5 of the Supporting Information. There were no data available in the literature on indoor air concentrations of BP-12 and UV-328. These two substances were therefore only considered when calculating the temperature-dependent K_{OA} and estimating the partitioning between different compartments using example values (see Section 3.2).

The average concentrations SVOC indoor air reported in the literature were assumed to be the total airborne SVOC concentrations (gas phase and particle phase) in the test house under the current climatic conditions (by 2020). It was assumed that the nine selected SVOCs originate from indoor sources that emit constantly during the period under consideration (see Section 3.3 for a detailed discussion). The emission rates (see Table 2) were calculated using equation 1 to obtain simulated concentrations that are within the approximate range (orders of magnitude) of the literature values for each SVOC.

2.4.2. SVOC Partitioning Indoors. Several studies have shown that assuming an instantaneous equilibrium can lead to large errors in estimating indoor SVOC concentrations.^{23,84,85} Therefore, in this work, the evaluation of SVOC partitioning is treated as a postprocessing module. The partitioning of SVOCs can occur between the gas phase, airborne particles, house dust, clothing, surfaces of furniture and interior walls of buildings, and even the skin of humans (and animals).²³

The ratio between the concentration of an SVOC in the particle phase and in the gas phase can be quantified by the particle/gas partition coefficient (K_p , m³ μg⁻¹) and the total suspended particle concentration [TSP], as described in equation 10.^{31,32,86}

$$\frac{F}{C_g} = [\text{TSP}] \cdot K_p \quad (10)$$

F and C_g are the particle-phase and gas-phase concentrations of the substance, respectively. The proportion of molecules sorbed on the particles Φ can therefore be calculated as follows (eq 11):

$$\Phi = \frac{F}{C_g + F} = \frac{K_p \cdot [\text{TSP}]}{1 + K_p \cdot [\text{TSP}]} \quad (11)$$

Table 3. $\log K_{OA}$ Values at 298 K Calculated in This Work and Literature Data

Compound	BP-12	BP-3	DINCH	DnBP	HHCB	PFOA	TCPP	UV-328	TPP	TXIB
$\log K_{OA}$ (this work)	11.12	8.33	10.86	9.05	8.21	6.7	9.38	10.18	11.28	7.51
$\log K_{OA}$ (literature)	10.57 ^a	9.06 ^b	-	8.84 ^a	7.85 ^b	4.16 ^a	9.92 ^b	10.57 ^a	10.09 ^b	7.44 ^a

^aOPERA (Mansouri et al., 2018).⁵⁸ ^bOkeme et al. (2020).⁵⁷

Table 4. Quantum-Mechanically Generated Temperature Dependent Logarithmic Octanol/Air Partition Coefficients ($\log K_{OA}$) of the 9 Target SVOCs and the Reference Compound DnBP

T (K)	$\log K_{OA}$									
	BP-12	BP-3	DINCH	DnBP	HHCB	PFOA	TCPP	UV-328	TPP	TXIB
283.15	11.97	8.96	11.74	9.74	8.88	7.52	10.14	10.98	12.12	8.16
288.15	11.68	8.74	11.43	9.50	8.65	7.24	9.88	10.70	11.83	7.93
293.15	11.40	8.53	11.14	9.27	8.43	6.96	9.63	10.44	11.55	7.71
298.15	11.12	8.33	10.86	9.05	8.21	6.70	9.38	10.18	11.28	7.51
303.15	10.86	8.14	10.59	8.83	8.01	6.45	9.15	9.93	11.03	7.31
308.15	10.61	7.95	10.33	8.63	7.81	6.21	8.92	9.70	10.78	7.11
313.15	10.37	7.77	10.08	8.43	7.62	5.98	8.71	9.47	10.54	6.93
318.15	10.14	7.60	9.84	8.24	7.44	5.76	8.50	9.25	10.31	6.75
323.15	9.91	7.44	9.61	8.06	7.26	5.55	8.30	9.04	10.09	6.58

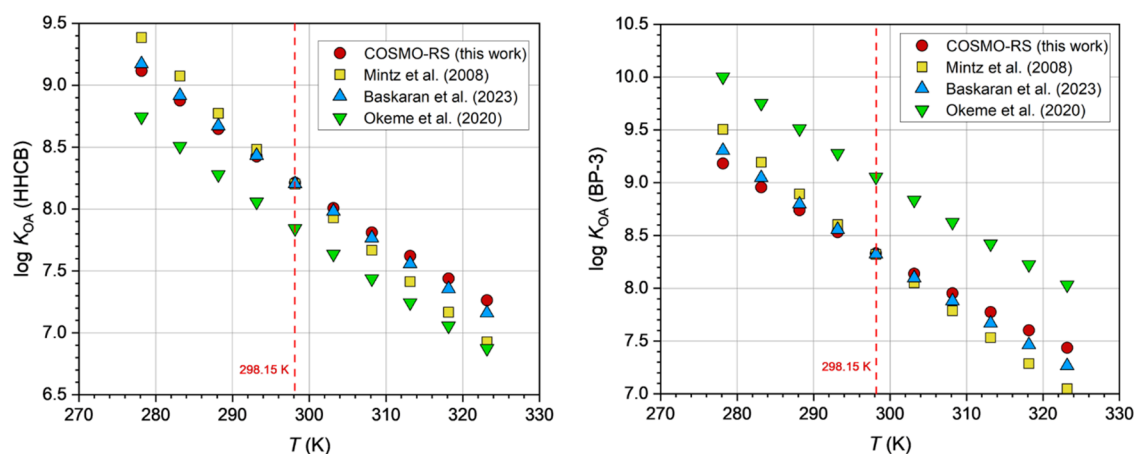


Figure 2. Temperature dependent $\log K_{OA}$ values for HHCB (left) and BP-3 (right). COSMO-RS data for HHCB: see Table 4; van't Hoff calculations for HHCB: Mintz et al.: $\log K_{OA}$ (298 K) = 8.21, $\Delta_{OA}H_i = 93.92$ kJ mol⁻¹; Baskaran et al.: $\log K_{OA}$ (298 K) = 8.21, $\Delta_{OA}U_i = 76.91$ kJ mol⁻¹; Okeme et al.: $\log K_{OA}$ (298 K) = 7.85, $\Delta_{OA}U_i = 71.5$ kJ mol⁻¹. COSMO-RS data for BP-3: see Table 4; van't Hoff calculations for BP-3: Mintz et al.: $\log K_{OA}$ (298 K) = 8.33, $\Delta_{OA}H_i = 85.59$ kJ mol⁻¹; Baskaran et al.: $\log K_{OA}$ (298 K) = 8.33, $\Delta_{OA}U_i = 77.96$ kJ mol⁻¹; Okeme et al.: $\log K_{OA}$ (298 K) = 9.06, $\Delta_{OA}U_i = 75.3$ kJ mol⁻¹.

K_p can be calculated from K_{OA} using the well-established approach by Finizio et al.^{32,31} Equation 12 assumes that the physical properties of octanol and the organic matter on particles are similar,^{87,89}

$$\log K_p = \log K_{OA} + \log f_{omp} - 11.91 \quad (12)$$

where f_{omp} is the fraction of organic matter in the particle phase. In this work $f_{omp} = 0.35$ is assumed⁸⁸ and the PM₁₀ concentration is used to represent the [TSP].

The gas/surface partitioning coefficient K_{surf} is defined according to equation 13 as the ratio of the concentration of an SVOC in the organic film of the surface (C_{surf}) and in the gas phase (C_g).

$$K_{surf} = \frac{C_{surf}}{C_g} \approx K_{OA} \quad (13)$$

Provided that the affinity of an SVOC to an organic film on a surface is similar to its affinity to 1-octanol, K_{surf} is then approximately equal to the K_{OA} of the SVOC.²³ Note that the C_{surf} refers to the surface-sorbed SVOC mass per volume of organic matter (V_{film}) on the surface film. Existing studies have mostly focused on smooth, impermeable surfaces such as window glass.^{89–92,94} The total area of

indoor window surfaces in the test house is 6.8 m² (see Table S3 of the Supporting Information). The reported effective thickness of organic films on indoor surfaces is typically between 5 and 30 nm.^{91,93} Weschler and Nazaroff⁹⁴ state that the thickness of the organic layer on a surface depends on various parameters and can only be estimated with considerable uncertainty. A smaller $\log K_{OA}$ value leads to a reduction in film thickness, but SVOCs with a small $\log K_{OA}$ equilibrate more rapidly with the surface. Since we cannot make any reasonable assumptions about the change in film thickness over time, and the surface area also varies from house to house, we estimate a value of 10 nm, resulting in $V_{film} = 6.8 \times 10^{-8}$ m³. The partitioning on other surfaces (e.g., human skin) was not included for simplicity.

Although it has been well researched for decades that SVOCs accumulate in house dust,⁹⁵ no conclusions can be drawn about the exposure of residents from house dust data. This is partly because of the unknown age of the house dust and the different methods used to collect and analyze samples, which makes it difficult to compare measurement results.⁹⁶ Nevertheless, we made predictions about the SVOC content in house dust as a function of $\log K_{OA}$ and the SVOC gas phase concentration. For space reasons, the details can be found in Section S2 of the Supporting Information.

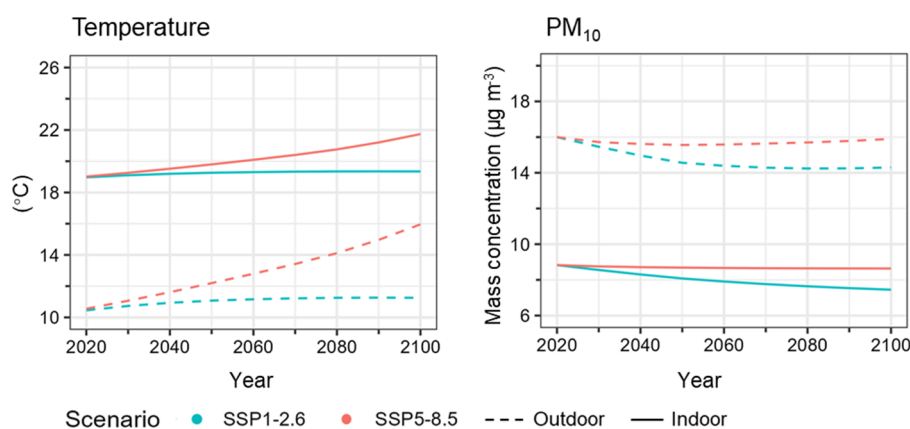


Figure 3. Annual average of temperature and PM₁₀ mass concentrations in the test house from 2020 to 2100 under two SSP climate scenarios. Outdoor data was based on IPCC projections, and indoor data was simulated by the IAQCC model.

3. RESULTS AND DISCUSSION

3.1. Temperature Dependent log K_{OA}

For the 10 compounds discussed here, log K_{OA} values were calculated using quantum mechanical methods in the temperature range from 283 to 323 K at intervals of 5 K. For 298 K, these log K_{OA} values were compared with literature data (see Table 3). Okeme et al.⁵⁷ provide experimental log K_{OA} at 298 K for BP-3, HHCB, TCPP, and TPP. The log K_{OA} values of the other substances at 298 K, available in the literature, were calculated using the QSAR (Quantitative Structure–Activity Relationship) tool OPERA (Open Quantitative Structure–activity/property Relationship App).⁵⁸

We find good agreement between our quantum-mechanically generated values for log K_{OA} with those of Okeme et al.⁵⁷ and OPERA,⁵⁸ respectively. Note that the temperature dependencies of the literature data were calculated using equation 9, applying the Baskaran et al.⁵⁵ method (eq 8) to calculate $\Delta_{OA}U_i$ for the OPERA data. Since no significant deviations from the literature data were found, the quantum mechanically determined temperature-dependent log K_{OA} values (see Table 4) are used for predicting the partitioning of SVOCs as described in Section 3.2.

K_{OA} is sensitive to temperature, which is mainly due to the high enthalpies of phase transfer. At $\Delta_{OA}H_i = 60 \text{ kJ mol}^{-1}$, K_{OA} changes by a factor of 2.4 and at $\Delta_{OA}H_i = 100 \text{ kJ mol}^{-1}$ by a factor of 4.0 per 10 degrees change of temperature.⁵¹ $\Delta_{OA}U_i$ is obtained from $\Delta_{OA}H_i$ using equation 6. However, with $\approx 2.5 \text{ kJ mol}^{-1}$ at 298 K, $R \cdot T$ is small compared to $\Delta_{OA}H_i$ and is therefore often neglected.⁵¹ Higher temperatures promote transfer into the gas phase, therefore K_{OA} decreases with increasing temperature. It is also important whether the K_{OA} refers to dry or wet octanol, since the solubility of water in octanol also changes with temperature.⁹⁷ However, the differences are not very large and are essentially important for ionizable substances. This primarily concerns the strong acid PFOA with an acid dissociation constant $\text{p}K_a(300 \text{ K}) \approx -0.09$.⁹⁸ The other target compounds are nonionizable and have only weak donor and acceptor properties.

Figure 2 shows that for the substances HHCB and BP-3, COSMO-RS reproduces the temperature-dependent log K_{OA} values significantly better than it does for the vapor pressure (see Section S1.2 in the Supporting Information for vapor pressure data). The red bullets (●) represent the values calculated with COSMO-RS, the yellow squares (■), blue

triangles (▲), and green triangles (▼) represent the results of the van't Hoff equation 4 with $\Delta_{OA}H_i$ according to Mintz et al.,⁵⁴ $\Delta_{OA}U_i$ according to Baskaran et al.,⁵⁵ and the experimental data of Okeme et al.⁵⁷

The deviations between the log K_{OA} values at 298 K determined experimentally or calculated using different methods are within the expected range. There is no significant difference between the experimentally based van't Hoff data of Okeme et al.⁵⁷ and the COSMO-RS data. From linear regression of the logarithmic COSMO-RS data against $1/T$ and under consideration of $R \cdot T$ we obtain $\Delta_{OA}U_i = 71 \text{ kJ mol}^{-1}$ for BP-3 and $\Delta_{OA}U_i = 73 \text{ kJ mol}^{-1}$ for HHCB. Good $\Delta_{OA}U_i$ agreements were also obtained for TPP and TCPP. However, the calculation of $\Delta_{OA}H_i$ according to Mintz et al.⁵⁴ leads to significantly higher values than the $\Delta_{OA}U_i$ of Baskaran et al.⁵⁵ and Okeme et al.,⁵⁷ which is reflected in a steeper slope of these data.

3.2. Long-Term Prediction of Indoor SVOC Partitioning

As described in Section 2.4.2, the prediction of SVOC partitioning in the test house considers the gas phase, the particle phase and indoor surfaces. Results of long-term predictions (2020 to 2100) of indoor climate and particle concentrations in the test houses are summarized in Figure 3 as annual averages, including two IPCC climate scenarios: SSP1–2.6 and SSP5–8.5. The future indoor temperature will increase due to increasing outdoor temperature and solar radiation. Depending on the scenario, the IPCC predicts a decreasing trend in future outdoor particle concentrations due to legislation on air pollution that has already been or will be implemented. Accordingly, the simulated indoor PM₁₀ concentration also shows a decreasing trend. Note that the European Community will adopt the air quality guidelines of the World Health Organization (WHO)⁹⁹ from 2030 onward (EU Directive 2024/2881, adopted on 23 October 2024). As shown in Figure 3, the temperature increase under scenario SSP5–8.5 is more pronounced than under SSP1–2.6, while the PM₁₀ mass concentration shows a greater decrease under SSP1–2.6 than under SSP5–8.5.

As already mentioned in Section 2.1 and Section 2.3, our model includes a building physics simulation that takes ambient weather conditions into account. Therefore, rather than using a constant annual mean, the model applies weather data with full annual cycle variations (for example, see annual temperature cycle for 2100 in Section S3 of the Supporting

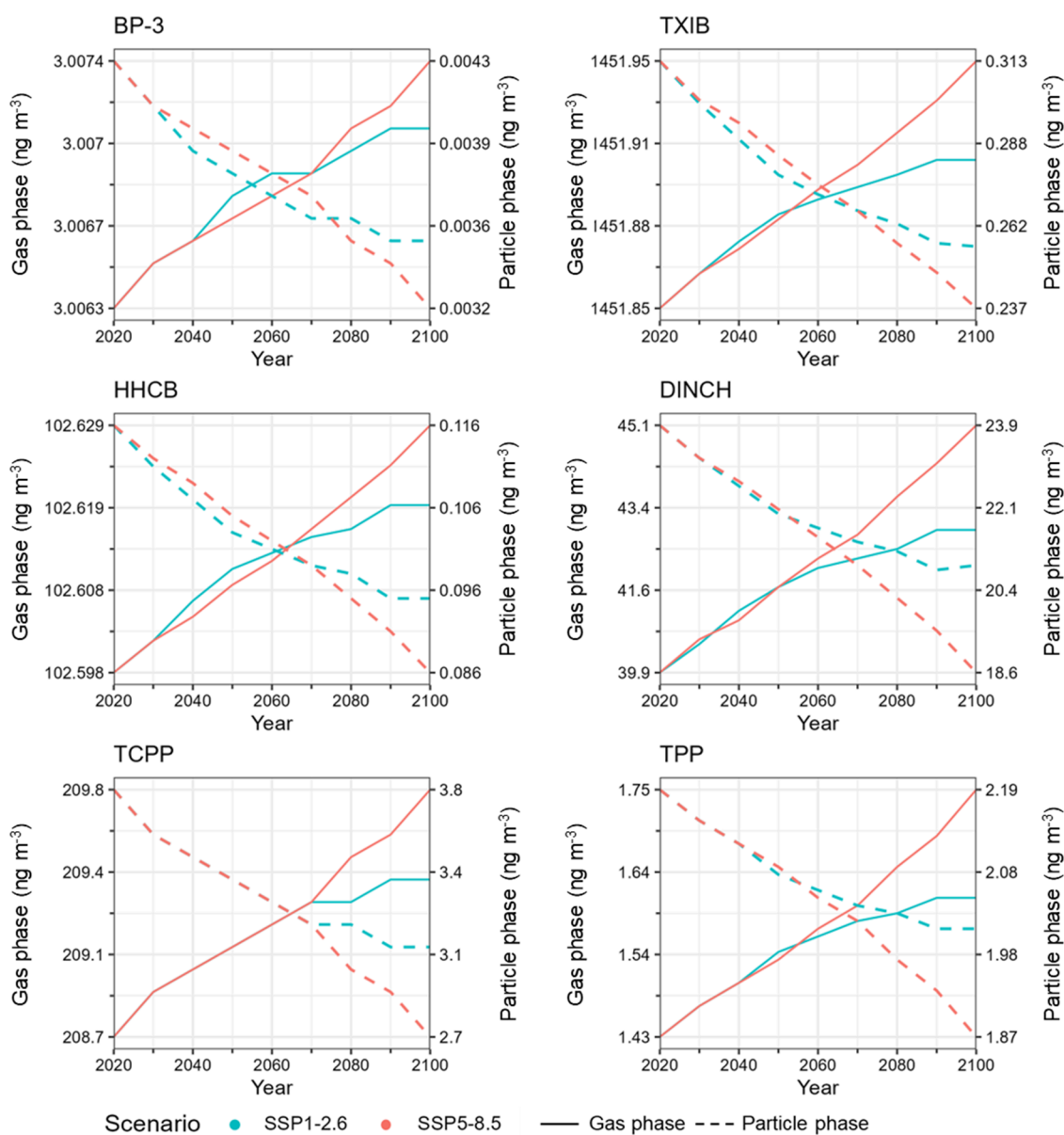


Figure 4. Predicted annual gas phase and particle phase concentrations of six SVOCs in indoor air of the test house in the time period from 2020 to 2100 under two SSP climate scenarios. Note that the units and decimal places shown on the *y*-axis are due to the calculations and are not necessarily related to any practically measurable values.

Information). Accordingly, temperature-dependent $\log K_{OA}$ values were applied in the simulation of SVOC partitioning.

Based on the simulated indoor temperature and PM_{10} concentrations in the test house, the long-term trend of gas/particle partitioning of SVOCs is illustrated in Figure 4. Due to a lack of data, BP-12 and UV-328 could not be included. The simulation results for PFOA are also not displayed due to the low concentrations and extremely small changes in the gas phase concentration (increase of $7 \times 10^{-7} \text{ ng m}^{-3}$ and $2 \times 10^{-6} \text{ ng m}^{-3}$ from $0.0708342 \text{ ng m}^{-3}$ under scenarios SSP1-2.6 and SSP5-8.5, respectively).

In both scenarios (SSP1-2.6 and SSP5-8.5), the gas phase concentrations tend to increase and the particle phase concentrations tend to decrease. Under the SSP1-2.6 scenario, the annual increase in gas phase concentrations ranges from 0.001% (PFOA) to 13% (TPP), and the annual decrease in particle phase concentrations ranges from 8% (TPP) to 19% (PFOA). Under the SSP5-8.5 scenario, the

annual increase in gas phase concentrations ranges from 0.003% (PFOA) to 22% (TPP), and the annual decrease in particle phase concentrations ranges from 15% (TPP) to 30% (PFOA).

Overall, the concentrations in the gas and particle phase show greater changes in scenario SSP5-8.5 than in scenario SSP1-2.6. According to eqs 11 and 12, the partitioning of SVOCs is governed by the temperature-dependent K_{OA} and the content of organic matter in particles. The increasing temperature leads to a lower $\log K_{OA}$ (Table 4), and thus to a lower K_p and a lower proportion of molecules Φ sorbed to the particles. The decreasing PM_{10} concentration further reduces the Φ value. Both parameters thus contribute to a change in the gas/particle equilibrium. For $f_{omp} = 0.35$ and $PM_{10} = 10 \mu\text{g m}^{-3}$ is $\Phi = 0.30$ at $\log K_{OA} = 11$ and $\Phi = 0.04$ at $\log K_{OA} = 10$. For $PM_{10} = 5 \mu\text{g m}^{-3}$ is $\Phi = 0.18$ at $\log K_{OA} = 11$ and $\Phi = 0.02$ at $\log K_{OA} = 10$.

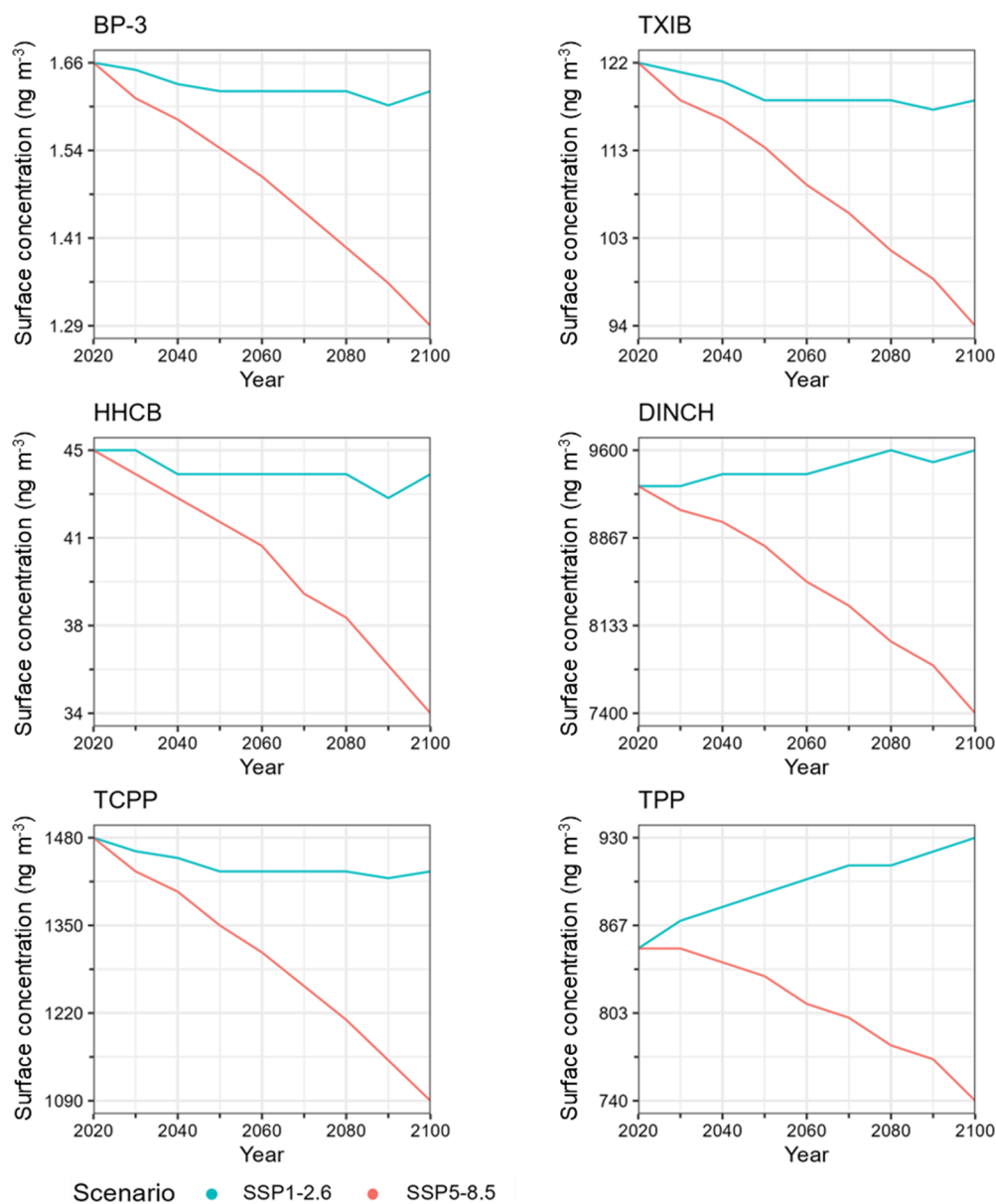


Figure 5. Predicted annual concentrations of six SVOCs sorbed on indoor surfaces of the test house in the time period from 2020 to 2100 under two SSP climate scenarios.

Among all selected SVOCs, TPP has the highest and PFOA the lowest $\log K_{OA}$. Consequently, according to eqs 3 and 4 the particle-to-gas phase concentration ratio is highest for TPP and lowest for PFOA, which agrees with the results shown in Figure 4. DINCH also has a high mass fraction in the particle phase; the same applies to BP-12, which is not shown in Figure 4. All other SVOCs, including UV-328, exhibit significantly higher concentrations in the gas phase than in the particle phase.

It must be stated clearly that this discussion describes aspects which, based on theoretical principles, are certainly correct. However, in some cases, such as the gas phase and particle phase concentrations of BP-3, TXIB, and HHCB, the changes are even less than 0.1 ng m^{-3} and thus below the detection or resolution limits of standard measurement methods, making them insignificant from a measurement perspective.

The amount of SVOCs sorbed on indoor surfaces was calculated using the simulated gas phase concentrations according to eq 13. The long-term trend of SVOCs on indoor surfaces in the test house is illustrated in Figure 5. Since the thickness of the organic layer on a solid indoor surface was assumed to be constant at 10 nm (see Section 2.4.2), the changes are determined by the gas phase concentrations of the SVOC and the corresponding temperature-dependent K_{OA} . Figure 5 indicates a decreasing trend for the concentrations of most of the target SVOCs on indoor surfaces. This means that the decrease in K_{OA} due to the temperature increase outweighs the effect of the projected increase in SVOC concentrations in the gas phase. In scenario SSP5–8.5, the decrease in surface concentration ranges from 13% for TPP to 28% for PFOA.

Figure 6 further demonstrates the temperature-dependent partitioning of SVOCs between gas phase, particle phase and indoor surfaces. PFOA ($\log K_{OA}$ between approximately 5.5 and 7.5), UV-328 ($\log K_{OA}$ between approximately 9 and 11)

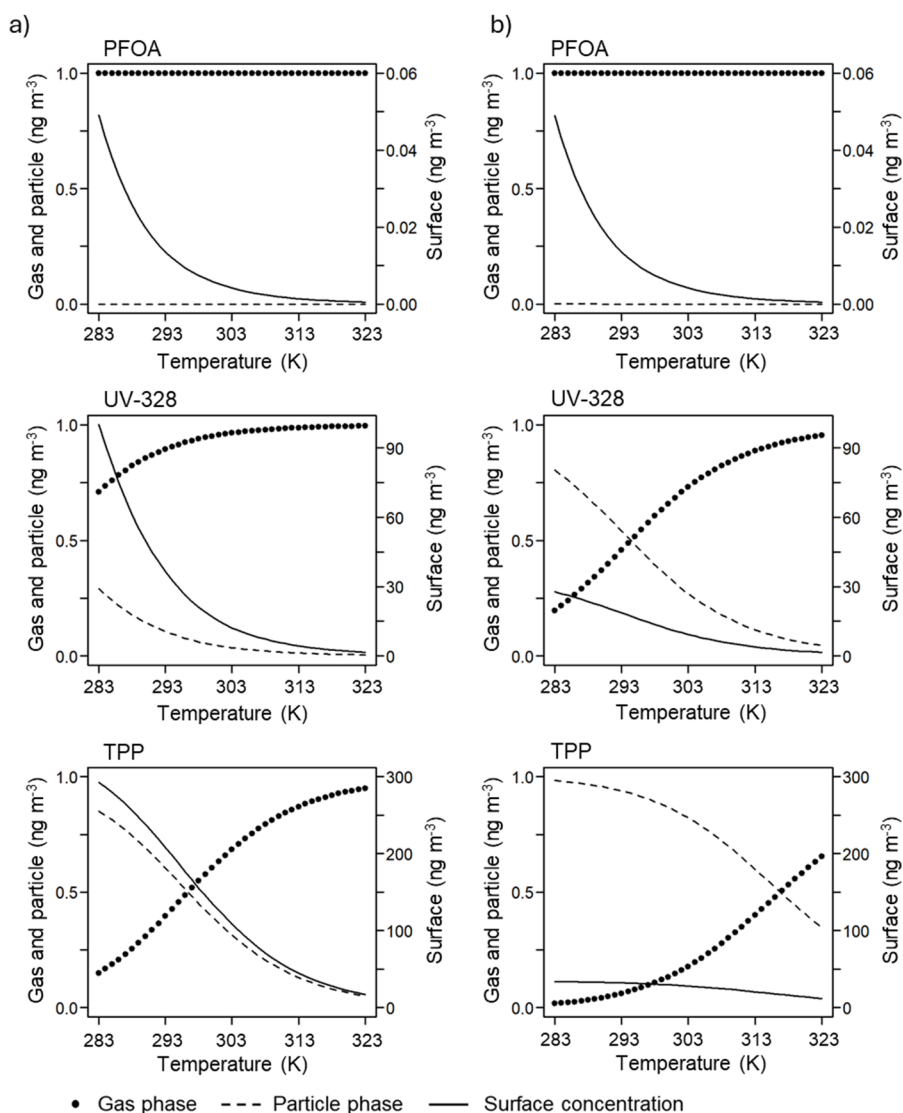


Figure 6. Temperature-dependent partitioning of PFOA, UV-328 and TPP between gas phase, particle phase and indoor surfaces at an air concentration (gas + particle) of 1 ng m^{-3} under test house conditions and PM_{10} concentrations of $10 \text{ } \mu\text{g m}^{-3}$ (Figure 6a) and $100 \text{ } \mu\text{g m}^{-3}$ (Figure 6b).

and TPP ($\log K_{\text{OA}}$ between approximately 10 and 12) were selected as examples, representing the low, medium and high K_{OA} range of SVOCs. For a better comparison, it was assumed that the air concentrations of these three compounds are the same (1 ng m^{-3}) and that the PM_{10} concentration is constant at either $10 \text{ } \mu\text{g m}^{-3}$ or $100 \text{ } \mu\text{g m}^{-3}$.

In the case of PFOA, the proportion in the gas phase is consistently around 100% in the investigated temperature range between 283 and 323 K. For UV-328 and TPP, higher proportions in the particle phase and higher concentrations on surfaces in indoor environments are observed due to the higher K_{OA} values.

The particle concentration also influences the fraction of SVOCs in the gas and particle phase. At a PM_{10} concentration of $10 \text{ } \mu\text{g m}^{-3}$, as shown in Figure 6a, UV-328 is almost 100% present in the gas phase at temperatures above 303 K. The same applies to TPP at temperatures above 323 K. At a PM_{10} concentration of $100 \text{ } \mu\text{g m}^{-3}$ (see Figure 6b) the equilibrium of UV-328 and TPP is shifted further toward the particle phase as predicted by eq 11, while the fraction sorbed on surfaces is

significantly smaller and continues to decrease with increasing temperature. For DINCH and BP-12, the $\log K_{\text{OA}}$ value is between approximately 10 and 12; therefore, the partitioning behavior of these substances is likely similar to that of TPP. BP-3, HHCb, TCPP, and TXIB are in the range between PFOA and UV-328.

For purposes of comparison, the DnBP concentration in the gas and particle phase was also calculated and compared with literature data. Occurrence and dynamics of DnBP indoors have been well researched, literature studies include countries in Europe, Asia, and the US, with indoor DnBP air concentrations between $0.1 \text{ } \mu\text{g m}^{-3}$ and $7 \text{ } \mu\text{g m}^{-3}$.^{14–16,100–104} Among these, the data in Blanchard et al.¹⁵ was used for comparison, as it was measured in European households (30 French homes) and reported the measured DnBP both in the gas phase (median concentration 83 ng m^{-3}) and in the particle phase (median concentration 17 ng m^{-3}) in each household. The sum of gas and particle concentrations was treated as total air concentration of DnBP in the simulation. Assuming an indoor temperature of 293 K

and a PM_{10} concentration of $30 \mu\text{g m}^{-3}$, the simulated DnBP concentrations in gas and particle phase were 97.7 ng m^{-3} and 2.3 ng m^{-3} , respectively. According to the measurement data in all households published by Blanchard et al.,¹⁵ the percentage of DnBP in the gas phase ranged from 17.6% to 97.5%, with a median of 85%. In this work, the simulated percentage of DnBP in the gas phase (97.7%) is at the upper end of the measured results. One reason can be attributed to the unknown particle concentration and composition, e.g. fraction of organic matter of the particle, in the respective households. With a higher particle concentration and a higher fraction of organic matter, a higher percentage of SVOCs in the particle phase can be expected. Another reason could be that the partitioning with house dust and the resuspension of house dust were not considered in our simulation.⁹⁴ Furthermore, in real-world conditions, the particles being transported from outdoor might already contain a specific amount of SVOCs.^{105,106}

3.3. Influence of Temperature and Humidity on SVOC Partitioning

Forecasts of future climate primarily consider temperature, but the impact of humidity on air quality is often overlooked. However, the high heat capacity of water essentially determines the enthalpy of air,¹⁰⁷ and the donor/acceptor properties of the water molecule influence chemical reactions and dynamic processes. For example, formaldehyde emission from urea-formaldehyde bonded particleboard is strongly influenced by air humidity.¹⁰⁸ Similarly, air humidity influences particle formation. The temperature dependence of the limonene/ozone reaction is well described,¹⁰⁹ but Jonsson et al.¹¹⁰ later showed that the yield of SOA at constant temperature increases with increasing humidity. This effect is presumably due to the reaction of water with the acidic reaction products and cannot be generalized.

Our model is capable of simulating coupled heat and moisture transfer through the building envelope (see our previous publications by Zhao et al.³ and Salthammer et al.⁴³). In this work, we applied projection data on future climate scenarios provided by IPCC WGI Atlas^{75,76} for the region of Western and Central Europe, where the test house is located (see Table S4 in the Supporting Information). However, these projections indicate no significant change in precipitation by 2100 (only a 0.5% increase under the SSP5–8.5 scenario), implying that major shifts in regional humidity levels are unlikely.

Regarding the influence of humidity on SVOC partitioning and emissions, the available literature is limited, and existing studies suggest that humidity effects are generally less important than temperature effects. Clausen et al.¹¹¹ experimentally demonstrated that humidity has little impact on the emission of di-2-ethylhexyl phthalate (DEHP) from PVC flooring. Zhou et al.³⁶ investigated the effects of temperature and humidity on gas–particle partitioning of phthalate esters and reported that humidity exerted a smaller influence on the gas/particle partition coefficient than temperature, with no clear trend. These results are understandable, as phthalates exhibit hardly any donor or acceptor properties. With the exception of PFOA, this also applies to the target molecules considered here. PFOA is an acid; therefore, its proportion in the particle phase increases with increasing humidity and decreasing organic content of the particles.⁵¹

Data describing the quantitative relationship between emission rates and temperature are available only for a limited number of SVOCs and indoor materials.^{35,36,112,113} Xiong et al.¹¹³ used an empirical equation to investigate the temperature-dependent emission behavior of DEHP from vinyl flooring. Liang and Xu¹¹² determined the phase change enthalpies from materials for various plasticizers and found that these do not correlate with the evaporation enthalpies. This generally makes it difficult to predict the temperature dependence of SVOC emissions from solid materials. It is clear that the surface area-specific emission rate (SE_{RA}) of an SVOC from a specific material tends to increase with increasing temperature. On the other hand, products become lower emitting through improved source control. Therefore, we assumed constant emission rates for the target SVOCs in the long term simulations (see Section 2.4.1).

Among the compounds examined in this study, temperature-dependent emission data are available only for DINCH, which were reported by Liang and Xu.¹¹² Based on these data, we have performed additional simulations for DINCH in the test house that incorporate temperature-dependent emission rates from a mattress cover (see Section S3 of the Supporting Information). The results predict an average annual total concentration of 100 ng m^{-3} for airborne DINCH by 2100. This value is approximately 1.6 times higher than the concentration of 64 ng m^{-3} calculated using a constant emission rate for DINCH (see Table 2 and Figure 4). Due to the many simplifying assumptions and uncertainties of the empirical model by Xiong et al.,¹¹³ we do not consider this difference in the annual average to be statistically significant. However, the simulation also shows that the trend for SVOC concentrations is a moderate increase in the annual average, while high peak concentrations may be reached on individual hot days (see Figure S3 in the Supporting Information).

4. CONCLUSIONS

As shown in previous work,^{3,42} climate change will lead to increasing indoor temperatures and, thus, to altered concentrations and partitioning of indoor pollutants, depending on the respective future climate scenario. The present study focuses on selected SVOCs that are widely used in building materials and consumer goods and will continue to be relevant in the future. Based on currently available literature data, we use our IAQCC model to predict the trends of SVOC indoor concentrations for the coming decades. Regarding the partitioning of SVOCs in the three investigated compartments (gas phase, airborne particles, and solid surfaces), different behaviors were observed under the conditions of the test house and the selected SSP climate scenarios SSP1–2.6 and SSP5–8.5.

With the aid of a quantum mechanical approach, we were able to accurately calculate temperature-dependent octanol/air partition coefficients K_{OA} and subcooled liquid vapor pressures P_L of the target SVOCs across typical indoor temperature ranges. Such reliable data provide the necessary basis for reasonable simulations of the dynamics of SVOCs in indoor environments.

As expected, the predicted $\log K_{OA}$ values decrease with increasing temperature (see Table 4). This means that, under the influence of climate change, rising indoor temperatures will lead to higher gas phase concentrations and lower amounts of SVOCs sorbed to airborne particles and surfaces. At the same time, it must be considered that, according to IPCC

projections,⁷⁶ the concentration of airborne particles are expected to decrease in the future. This will also decrease the amount of SVOCs sorbed to the particle phase. These two combined effects are clearly visible in the long term simulation results for the target SVOCs in the test house (see Figure 4). Scenario SSP5–8.5 leads to a greater temperature increase and a smaller decrease in particle concentration than scenario SSP1–2.6. Consequently, larger changes are observed in scenario SSP5–8.5 than in scenario SSP1–2.6. This suggests that, according to current climate trends, temperature changes have a greater impact on indoor SVOC concentrations than changes in particle concentrations.

Our study is primarily limited by the fact that the simulations for the partitioning of SVOCs only considered three compartments with simplified assumptions. For example, a constant organic film thickness of 10 nm was assumed on indoor surfaces. In reality, the properties of the organic film can be influenced by temperature, humidity, particle deposition, chemical reactions, and the characteristics of indoor materials.^{94,114} Existing studies have mostly focused on smooth, impermeable surfaces such as window glass and metal objects.^{89–92} Additionally, routine cleaning and the replacement of furnishings over long time scales are expected to reduce film thickness.⁸⁹ Incorporating detailed film growth dynamics, including the influence of various environmental and material-related factors, is certainly desirable, but encounters practical limitations. For example, film formation for substances with high log K_{OA} occurs very slowly.⁹⁴ Similarly, the time factor plays a crucial role in the equilibration of SVOCs between gaseous phases and house dust.²³

The long-term simulations in this work are therefore not intended to precisely predict the partitioning of SVOCs within the building. The period between 2020 and 2100 is too long for this, and the calculated values are subject to corresponding uncertainties. This applies in particular to the discussed influences of temperature and humidity. Rather, our results provide meaningful estimates of long-term trends under both optimistic and pessimistic scenarios regarding future climate conditions. The SVOC data discussed here were obtained using our IAQCC model⁴³ and supplemented by previous findings on indoor climate and indoor air quality. We believe this work will contribute to better preparing and designing indoor spaces for the anticipated impacts of climate change to ensure adequate protection for occupants.^{4,43}

■ ASSOCIATED CONTENT

■ Supporting Information

The Supporting Information is available free of charge at <https://pubs.acs.org/doi/10.1021/acsestair.5c00399>.

Experimentally determined and calculated Abraham descriptors from the UFZ database for the SVOCs selected in this study; log K_{OA} enthalpies of phase transfer $\Delta_{OA}H_i$ and internal energies of phase transfer $\Delta_{OA}U_i$ at 298 K; log K_{OA} enthalpies of phase transfer model input parameters for the test house used in this study; temperature, ozone concentration and $PM_{2.5}$ concentration in outdoor air under selected SSP scenarios; indoor air and dust concentrations of selected SVOCs; calculation method of temperature dependence of the vapor pressure; evaluation of calculated vapor pressures; partitioning of SVOCs between air and house

dust; temperature influence on SVOC emission rates (PDF)

■ AUTHOR INFORMATION

Corresponding Author

Alexandra Schieweck – Department of Material Analysis and Indoor Chemistry, Fraunhofer WKI, 38108 Braunschweig, Germany; orcid.org/0000-0003-2523-9934; Phone: +49-531-2155-924; Email: alexandra.schieweck@wki.fraunhofer.de

Authors

Jiangyue Zhao – Department of Material Analysis and Indoor Chemistry, Fraunhofer WKI, 38108 Braunschweig, Germany; orcid.org/0000-0001-5202-239X

Tunga Salthammer – Department of Material Analysis and Indoor Chemistry, Fraunhofer WKI, 38108 Braunschweig, Germany; orcid.org/0000-0002-2370-8664

Erik Uhde – Department of Material Analysis and Indoor Chemistry, Fraunhofer WKI, 38108 Braunschweig, Germany

Lukas Wittmann – Mulliken Center for Theoretical Chemistry, Institute for Physical and Theoretical Chemistry, University of Bonn, 53115 Bonn, Germany; orcid.org/0009-0008-9915-083X

Complete contact information is available at: <https://pubs.acs.org/10.1021/acsestair.5c00399>

Notes

The authors declare no competing financial interest.

■ ACKNOWLEDGMENTS

This work was supported by the Federal Ministry for the Environment, Nature Conservation, Nuclear Safety and Consumer Protection (BMUV), Germany [grant number REFOPLAN FKZ 3719 51 205 0]. The authors greatly acknowledge the granted access to the Marvin cluster hosted by the University of Bonn. L. Wittmann would like to express his deepest gratitude to Prof. Stefan Grimme for his exceptional support. L. Wittmann also greatly acknowledges support of the Stiftung Stipendien-Fonds des Verbandes der Chemischen Industrie e.V. through its Kekulé Fellowship program.

■ REFERENCES

- (1) Copernicus Climate Change Service, Copernicus: 2024 is the first year to exceed 1.5 °C above pre-industrial level, https://climate.copernicus.eu/copernicus-2024-first-year-exceed-15degc-above-pre-industrial-level?utm_source=chatgpt.com.
- (2) Weschler, C. J.; Carslaw, N. Indoor chemistry. *Environ. Sci. Technol.* **2018**, *52*, 2419–2428.
- (3) Zhao, J.; Uhde, E.; Salthammer, T.; Antretter, F.; Shaw, D.; Carslaw, N.; Schieweck, A. Long-term prediction of the effects of climate change on indoor climate and air quality. *Environ. Res.* **2024**, *243*, 117804.
- (4) Zeng, Z.; Song, B.; Xiao, R.; Zeng, G.; Gong, J.; Chen, M.; Xu, P.; Zhang, P.; Shen, M.; Yi, H. Assessing the human health risks of perfluorooctane sulfonate by in vivo and in vitro studies. *Environ. Int.* **2019**, *126*, 598–610.
- (5) Låg, M.; Øvrevik, J.; Refsnes, M.; Holme, J. A. Potential role of polycyclic aromatic hydrocarbons in air pollution-induced non-malignant respiratory diseases. *Respir. Res.* **2020**, *21*, 299.
- (6) Patisaul, H. B.; Roberts, S. C.; Mabrey, N.; McCaffrey, K. A.; Gear, R. B.; Braun, J.; Belcher, S. M.; Stapleton, H. M. Accumulation

and endocrine disrupting effects of the flame retardant mixture Firemaster® 550 in rats: An exploratory assessment. *J. Biochem. Mol. Toxicol.* **2013**, *27*, 124–136.

(7) Straif, K.; Baan, R.; Grosse, Y.; Secretan, B.; El Ghissassi, F.; Coglianò, V. Carcinogenicity of polycyclic aromatic hydrocarbons. *Lancet Oncol.* **2005**, *6*, 931–932.

(8) Deng, W. J.; Zheng, H. L.; Tsui, A. K.; Chen, X. W. Measurement and health risk assessment of PM(2.5), flame retardants, carbonyls and black carbon in indoor and outdoor air in kindergartens in Hong Kong. *Environ. Int.* **2016**, *96*, 65–74.

(9) WHO, *Literature review on chemical pollutants in indoor air in public settings for children and overview of their health effects with a focus on schools, kindergartens and day-care centres*; World Health Organization, Regional Office for Europe, Copenhagen, 2021.

(10) Krause, M.; Klit, A.; Blomberg Jensen, M.; Søbørg, T.; Frederiksen, H.; Schlumpf, M.; Lichtensteiger, W.; Skakkebaek, N. E.; Drzewiecki, K. T. Sunscreens: are they beneficial for health? An overview of endocrine disrupting properties of UV-filters. *Int. J. Androl.* **2012**, *35*, 424–436.

(11) Landeg-Cox, C.; Middleton, A.; Halios, C.; Marczylo, T.; Dimitroulopoulou, S. Chemicals in European residences—Part II: A review of emissions, concentrations, and health effects of semi-volatile organic compounds (SVOCs). *Environments* **2025**, *12*, 40.

(12) Salvito, D. Synthetic musk compounds and effects on human health? *Environ. Health Perspect.* **2005**, *113*, A802–A803.

(13) Barreca, S.; Mancuso, M. M. M.; Sacristán, D.; Pace, A.; Savoca, D.; Orecchio, S. Determination of perfluorooctanoic acid (PFOA) in the indoor dust matter of the Sicily (Italy) area: analysis and exposure evaluations. *Toxics* **2024**, *12*, 28.

(14) Bergh, C.; Magnus Åberg, K.; Svartengren, M.; Emenius, G.; Östman, C. Organophosphate and phthalate esters in indoor air: a comparison between multi-storey buildings with high and low prevalence of sick building symptoms. *J. Environ. Monit.* **2011**, *13*, 2001–2009.

(15) Blanchard, O.; Glorennec, P.; Mercier, F.; Bonvallot, N.; Chevrier, C.; Ramalho, O.; Mandin, C.; Bot, B. L. Semivolatile organic compounds in indoor air and settled dust in 30 French dwellings. *Environ. Sci. Technol.* **2014**, *48*, 3959–3969.

(16) Fromme, H.; Lahrz, T.; Piloty, M.; Gebhart, H.; Oddoy, A.; Rüdten, H. Occurrence of phthalates and musk fragrances in indoor air and dust from apartments and kindergartens in Berlin (Germany). *Indoor air* **2004**, *14*, 188–195.

(17) Khare, A.; Jadhao, P.; Vaidya, A. N.; Kumar, A. R. Benzotriazole UV stabilizers (BUVs) as an emerging contaminant of concern: a review. *Environ. Sci. Pollut. Res.* **2023**, *30*, 121370–121392.

(18) Mao, J. F.; Li, W.; Ong, C. N.; He, Y.; Jong, M.-C.; Gin, K. Y.-H. Assessment of human exposure to benzophenone-type UV filters: a review. *Environ. Int.* **2022**, *167*, 107405.

(19) Plaisance, H.; Raffy, G.; Le Bot, B.; Bossanne, E.; Rawas, C.; Cardin, P.; Desauziers, V. Characteristics of tris(chloropropyl)-phosphate (TCPP) emission from upholstered furniture in offices and consequence on indoor air quality. *Build. Environ.* **2022**, *219*, 109156.

(20) Wan, Y.; Xue, J.; Kannan, K. Occurrence of benzophenone-3 in indoor air from Albany, New York, USA, and its implications for inhalation exposure. *Sci. Total Environ.* **2015**, *537*, 304–308.

(21) Venier, M.; Audy, O.; Vojta, Š.; Bečanová, J.; Romanak, K.; Melymuk, L.; Krátká, M.; Kukučka, P.; Okeme, J.; Saini, A.; Diamond, M. L.; Klánová, J. Brominated flame retardants in the indoor environment — Comparative study of indoor contamination from three countries. *Environ. Int.* **2016**, *94*, 150–160.

(22) Lucattini, L.; Poma, G.; Covaci, A.; de Boer, J.; Lamoree, M. H.; Leonards, P. E. G. A review of semi-volatile organic compounds (SVOCs) in the indoor environment: occurrence in consumer products, indoor air and dust. *Chemosphere* **2018**, *201*, 466–482.

(23) Weschler, C. J.; Nazaroff, W. W. Semivolatile organic compounds in indoor environments. *Atmos. Environ.* **2008**, *42*, 9018–9040.

(24) Wang, C.; Eichler, C. M. A.; Bi, C.; Delmaar, C. J. E.; Xu, Y.; Little, J. C. A rapid micro chamber method to measure SVOC emission and transport model parameters. *Environ. Sci.: Processes Impacts* **2023**, *25*, 818–831.

(25) Uhde, E.; Varol, D.; Mull, B.; Salthammer, T. Distribution of five SVOCs in a model room: effect of vacuuming and air cleaning measures. *Environ. Sci.: Processes Impacts* **2019**, *21*, 1353–1363.

(26) Liu, C.; Morrison, G. C.; Zhang, Y. Role of aerosols in enhancing SVOC flux between air and indoor surfaces and its influence on exposure. *Atmos. Environ.* **2012**, *55*, 347–356.

(27) Cox, S. S.; Little, J. C.; Hodgson, A. T. Predicting the emission rate of volatile organic compounds from vinyl flooring. *Environ. Sci. Technol.* **2002**, *36*, 709–714.

(28) Xu, Y.; Little, J. C. Predicting emissions of SVOCs from polymeric materials and their interaction with airborne particles. *Environ. Sci. Technol.* **2006**, *40*, 456–461.

(29) Xu, Y.; Cohen Hubal, E. A.; Clausen, P. A.; Little, J. C. Predicting residential exposure to phthalate plasticizer emitted from vinyl flooring: a mechanistic analysis. *Environ. Sci. Technol.* **2009**, *43*, 2374–2380.

(30) Junge, C. Basic considerations about trace constituents in the atmosphere as related to the fate of global pollutant. In *Advances in Environmental Science and Technology*, Suffet, I. H., Ed.; John Wiley & Sons: New York, 1977; pp 7–25.

(31) Pankow, J. F. Review and comparative analysis of the theories on partitioning between the gas and aerosol particulate phases in the atmosphere. *Atmos. Environ.* **1987**, *21*, 2275–2283.

(32) Finizio, A.; Mackay, D.; Bidleman, T.; Harner, T. Octanol-air partition coefficient as a predictor of partitioning of semi-volatile organic chemicals to aerosols. *Atmos. Environ.* **1997**, *31*, 2289–2296.

(33) Schripp, T.; Salthammer, T.; Fauck, C.; Bekö, G.; Weschler, C. J. Latex paint as a delivery vehicle for diethylphthalate and di-n-butylphthalate: predictable boundary layer concentrations and emission rates. *Sci. Total Environ.* **2014**, *494–495*, 299–305.

(34) Ni, Y.; Kumagai, K.; Yanagisawa, Y. Measuring emissions of organophosphate flame retardants using a passive flux sampler. *Atmos. Environ.* **2007**, *41*, 3235–3240.

(35) Clausen, P. A.; Liu, Z.; Kofoed-Sørensen, V.; Little, J.; Wolkoff, P. Influence of temperature on the emission of di-(2-ethylhexyl)-phthalate (DEHP) from PVC flooring in the emission cell FLEC. *Environ. Sci. Technol.* **2012**, *46*, 909–915.

(36) Zhou, X.; Lian, J.; Cheng, Y.; Wang, X. The gas/particle partitioning behavior of phthalate esters in indoor environment: effects of temperature and humidity. *Environ. Res.* **2021**, *194*, 110681.

(37) Pankow, J. F. An absorption model of gas/particle partitioning of organic compounds in the atmosphere. *Atmos. Environ.* **1994**, *28*, 185–188.

(38) Wei, W.; Mandin, C.; Blanchard, O.; Mercier, F.; Pelletier, M.; Le Bot, B.; Glorennec, P.; Ramalho, O. Temperature dependence of the particle/gas partition coefficient: an application to predict indoor gas-phase concentrations of semi-volatile organic compounds. *Sci. Total Environ.* **2016**, *563–564*, 506–512.

(39) Salthammer, T.; Goss, K.-U. Predicting the gas/particle distribution of SVOCs in the indoor environment using poly parameter linear free energy relationships. *Environ. Sci. Technol.* **2019**, *53*, 2491–2499.

(40) Stahn, M.; Grimme, S.; Salthammer, T.; Hohm, U.; Palm, W.-U. Quantum chemical calculation of the vapor pressure of volatile and semi volatile organic compounds. *Environ. Sci.: Processes Impacts* **2022**, *24*, 2153–2166.

(41) Salthammer, T.; Grimme, S.; Stahn, M.; Hohm, U.; Palm, W.-U. Quantum chemical calculation and evaluation of partition coefficients for classical and emerging environmentally relevant organic compounds. *Environ. Sci. Technol.* **2022**, *56*, 379–391.

(42) Zhao, J.; Salthammer, T.; Schieweck, A.; Uhde, E.; Hussein, T. Long-term prediction of climate change impacts on indoor particle pollution — case study of a residential building in Germany. *Environ. Sci.: Processes Impacts* **2025**, *27*, 1688–1703.

- (43) Salthammer, T.; Zhao, J.; Schieweck, A.; Uhde, E.; Hussein, T.; Antretter, F.; Künzel, H.; Pazold, M.; Radon, J.; Birmili, W. A holistic modeling framework for estimating the influence of climate change on indoor air quality. *Indoor air* **2022**, *32*, e13039.
- (44) Jenkin, M. E.; Saunders, S. M.; Pilling, M. J. The tropospheric degradation of volatile organic compounds: a protocol for mechanism development. *Atmos. Environ.* **1997**, *31*, 81–104.
- (45) Saunders, S. M.; Jenkin, M. E.; Derwent, R. G.; Pilling, M. J. Protocol for the development of the Master Chemical Mechanism, MCM v3 (Part A): Tropospheric degradation of non-aromatic volatile organic compounds. *Atmos. Chem. Phys.* **2003**, *3*, 161–180.
- (46) Hussein, T.; Korhonen, H.; Herrmann, E.; Hämeri, K.; Lehtinen, K. E. J.; Kulmala, M. Emission rates due to indoor activities: indoor aerosol model development, evaluation, and applications. *Aerosol Sci. Technol.* **2005**, *39*, 1111–1127.
- (47) Hussein, T.; Kulmala, M. Indoor aerosol modeling: basic principles and practical applications. *Water Air Soil Pollut.: Focus* **2008**, *8*, 23–34.
- (48) Hussein, T.; Wierzbicka, A.; Löndahl, J.; Lazaridis, M.; Hänninen, O. Indoor aerosol modeling for assessment of exposure and respiratory tract deposited dose. *Atmos. Environ.* **2015**, *106*, 402–411.
- (49) European Commission, Regulation (EC) No 1907/2006 of the European Parliament and of the Council, *Office Journal of the European Union*, 2006.
- (50) U.S. Consumer Product Safety Commission, Consumer Product Safety Improvement Act of 2008 (CPSIA), *Federal Register, Washington D.C.*, 2008.
- (51) Schwarzenbach, R. P.; Gschwend, P. M.; Imboden, D. M. *Environmental Organic Chemistry*; John Wiley & Sons, Hoboken, NJ, 2017.
- (52) Parnis, J. M.; Mackay, D. *Multimedia Environmental Models - The Fugacity Approach*; CRC Press, Boca Raton, FL, 2021.
- (53) Baskaran, S.; Duan Lei, Y.; Wania, F. Reliable prediction of the octanol-air partition ratio. *Environ. Toxicol. Chem.* **2021**, *40*, 3166–3180.
- (54) Mintz, C.; Burton, K.; Ladlie, T.; Clark, M.; Acree, W. E.; Abraham, M. H. Enthalpy of solvation correlations for gaseous solutes dissolved in dibutyl ether and ethyl acetate. *Thermochim. Acta* **2008**, *470*, 67–76.
- (55) Baskaran, S.; Podagatlapalli, A.; Sangion, A.; Wania, F. Predicting the temperature dependence of the octanol–air partition ratio: A new model for estimating $\Delta U^{0\text{oa}}$. *J. Solut. Chem.* **2023**, *52*, 51–69.
- (56) Ulrich, N.; Endo, S.; Brown, T. N.; Watanabe, N.; Bronner, G.; Abraham, M. H.; Goss, K.-U. *UFZ-LSER Database v 3.2.1. Helmholtz Centre for Environmental Research, Leipzig*, 2017.
- (57) Okeme, J. O.; Rodgers, T. F. M.; Parnis, J. M.; Diamond, M. L.; Bidleman, T. F.; Jantunen, L. M. Gas chromatographic estimation of vapor pressures and octanol–air partition coefficients of semivolatile organic compounds of emerging concern. *J. Chem. Eng. Data* **2020**, *65*, 2467–2475.
- (58) Mansouri, K.; Grulke, C. M.; Judson, R. S.; Williams, A. J. OPERA models for predicting physicochemical properties and environmental fate endpoints. *J. Cheminform.* **2018**, *10*, 10.
- (59) Bohle, F.; Seibert, J.; Grimme, S. Automated quantum chemistry-based calculation of optical rotation for large flexible molecules. *J. Org. Chem.* **2021**, *86*, 15522–15531.
- (60) de Souza, B. GOAT: A global optimization algorithm for molecules and atomic clusters. *Angew. Chem., Int. Ed.* **2025**, *64*, e202500393.
- (61) Bannwarth, C.; Ehlert, S.; Grimme, S. GFN2-xTB—An accurate and broadly parametrized self-consistent tight-binding quantum chemical method with multipole electrostatics and density-dependent dispersion contributions. *J. Chem. Theory Comput.* **2019**, *15*, 1652–1671.
- (62) Ehlert, S.; Stahn, M.; Spicher, S.; Grimme, S. Robust and efficient implicit solvation model for fast semiempirical methods. *J. Chem. Theory Comput.* **2021**, *17*, 4250–4261.
- (63) Grimme, S.; Bohle, F.; Hansen, A.; Pracht, P.; Spicher, S.; Stahn, M. Efficient quantum chemical calculation of structure ensembles and free energies for nonrigid molecules. *J. Phys. Chem. A* **2021**, *125*, 4039–4054.
- (64) Barone, V.; Cossi, M. Quantum calculation of molecular energies and energy gradients in solution by a conductor solvent model. *J. Phys. Chem. A* **1998**, *102*, 1995–2001.
- (65) Klamt, A.; Jonas, V.; Bürger, T.; Lohrenz, J. C. W. Refinement and parametrization of COSMO-RS. *J. Phys. Chem. A* **1998**, *102*, 5074–5085.
- (66) Katbashev, A.; Stahn, M.; Rose, T.; Alizadeh, V.; Friede, M.; Plett, C.; Steinbach, P.; Ehlert, S. Overview on building blocks and applications of efficient and robust extended tight binding. *J. Phys. Chem. A* **2025**, *129*, 2667–2682.
- (67) Neese, F. Software Update: The ORCA Program System—Version 6.0. *WIREs Computational Molecular Science* **2025**, *15*, e70019.
- (68) Wittmann, L.; Neugebauer, H.; Grimme, S.; Bursch, M. Dispersion-corrected r2SCAN based double-hybrid functionals. *J. Chem. Phys.* **2023**, *159*, 224103.
- (69) Stoychev, G. L.; Auer, A. A.; Neese, F. Automatic generation of auxiliary basis sets. *J. Chem. Theory Comput.* **2017**, *13*, 554–562.
- (70) Helmich-Paris, B.; de Souza, B.; Neese, F.; Izsák, R. An improved chain of spheres for exchange algorithm. *J. Chem. Phys.* **2021**, *155*, 104109.
- (71) Balasubramani, S. G.; Chen, G. P.; Coriani, S.; Diedenhofen, M.; Frank, M. S.; Franzke, Y. J.; Furche, F.; Grotjahn, R.; Harding, M. E.; Hättig, C.; Hellweg, A.; Helmich-Paris, B.; Holzer, C.; Huniar, U.; Kaupp, M.; Marefat Khah, A.; Karbalaei Khani, S.; Müller, T.; Mack, F.; Nguyen, B. D.; Parker, S. M.; Perlt, E.; Rappoport, D.; Reiter, K.; Roy, S.; Rückert, M.; Schmitz, G.; Sierka, M.; Tapavicza, E.; Tew, D. P.; van Wüllen, C.; Voora, V. K.; Weigend, F.; Wodyński, A.; Yu, J. M. TURBOMOLE: Modular program suite for ab initio quantum-chemical and condensed-matter simulations. *J. Chem. Phys.* **2020**, *152*, 184107.
- (72) Weigend, F.; Ahlrichs, R. Balanced basis sets of split valence, triple zeta valence and quadruple zeta valence quality for H to Rn: design and assessment of accuracy. *Phys. Chem. Chem. Phys.* **2005**, *7*, 3297–3305.
- (73) European Environment Agency, Air Quality e-Reporting, <https://www.eea.europa.eu/data-and-maps/data/aqereporting-9>, (accessed 02.03.2025).
- (74) Intergovernmental Panel on Climate Change, *Climate Change 2021: The Physical Science Basis*; Cambridge University Press, Cambridge, UK, 2021.
- (75) Iturbide, M.; Fernández, J.; Gutiérrez, J. M.; Pirani, A.; Huard, D.; Al Khourdajie, A.; Baño-Medina, J.; Bedia, J.; Casanueva, A.; Cimadevilla, E.; Cofiño, A. S.; De Felice, M.; Díez-Sierra, J.; García-Díez, M.; Goldie, J.; Herrera, D. A.; Herrera, S.; Manzanos, R.; Milovac, J.; Radhakrishnan, A.; San-Martín, D.; Spinuso, A.; Thyng, K. M.; Trenham, C.; Yelekçi, Ö. Implementation of FAIR principles in the IPCC: the WGI AR6 Atlas repository. *Sci. Data* **2022**, *9*, 629.
- (76) J.R.G. Gutiérrez, J. M.; Narisma, G. T.; Alves, L. M.; Amjad, M.; Gorodetskaya, I. V.; Grose, M.; Klutse, N. A. B.; Krakovska, S.; Li, J.; Martínez-Castro, D.; Mearns, L. O.; Mernild, S. H.; Ngo-Duc, T.; van den Hurk, B.; Yoon, J.-H., Atlas. In *Climate Change 2021: The Physical Science Basis. Contribution of Working Group I to the Sixth Assessment Report of the Intergovernmental Panel on Climate Change* (<http://interactive-atlas.ipcc.ch/>).
- (77) Fromme, H.; Schütze, A.; Lahrz, T.; Kraft, M.; Fembacher, L.; Siewering, S.; Burkardt, R.; Dietrich, S.; Koch, H. M.; Völkel, W. Non-phthalate plasticizers in German daycare centers and human biomonitoring of DINCH metabolites in children attending the centers (LUPE 3). *Int. J. Hyg. Environ. Health* **2016**, *219*, 33–39.
- (78) Giovanoulis, G.; Bui, T.; Xu, F.; Papadopoulou, E.; Padilla-Sanchez, J. A.; Covaci, A.; Haug, L. S.; Cousins, A. P.; Magnér, J.; Cousins, I. T.; de Wit, C. A. Multi-pathway human exposure assessment of phthalate esters and DINCH. *Environ. Int.* **2018**, *112*, 115–126.

- (79) Dodson, R. E.; Bessonneau, V.; Udesky, J. O.; Nishioka, M.; McCauley, M.; Rudel, R. A. Passive indoor air sampling for consumer product chemicals: a field evaluation study. *J. Expo. Sci. Environ. Epidemiol.* **2019**, *29*, 95–108.
- (80) Goosey, E.; Harrad, S. Perfluoroalkyl substances in UK indoor and outdoor air: spatial and seasonal variation, and implications for human exposure. *Environ. Int.* **2012**, *45*, 86–90.
- (81) Shoeib, M.; Harner, T.; Webster, G. M.; Lee, S. C. Indoor sources of poly- and perfluorinated compounds (PFCs) in Vancouver, Canada: implications for human exposure. *Environ. Sci. Technol.* **2011**, *45*, 7999–8005.
- (82) Marklund, A.; Andersson, B.; Haglund, P. Organophosphorus flame retardants and plasticizers in air from various indoor environments. *J. Environ. Monit.* **2005**, *7*, 814–819.
- (83) Umweltbundesamt (German Environment Agency), *Kinder-Umwelt-Survey 2003/06 - Innenraumluf*, Umweltbundesamt, Dessau-Roßlau, 2010.
- (84) Liu, C.; Shi, S.; Weschler, C.; Zhao, B.; Zhang, Y. Analysis of the dynamic interaction between SVOCs and airborne particles. *Aerosol Sci. Technol.* **2013**, *47*, 125–136.
- (85) Cao, J.; Mo, J.; Sun, Z.; Zhang, Y. Indoor particle age, a new concept for improving the accuracy of estimating indoor airborne SVOC concentrations, and applications. *Build. Environ.* **2018**, *136*, 88–97.
- (86) Pankow, J. F. An absorption model of the gas/aerosol partitioning involved in the formation of secondary organic aerosol. *Atmos. Environ.* **1994**, *28*, 189–193.
- (87) Bidleman, T. F.; Harner, T. Sorption to aerosols. In *Property Estimation Methods for Chemicals*, Boethling, R. S., Mackay, D., Eds.; Lewis Publishers: Boca Raton, 2000; Ch 10; pp 233–260.
- (88) Salthammer, T.; Schripp, T. Application of the Junge- and Pankow-equation for estimating indoor gas/particle distribution and exposure to SVOCs. *Atmos. Environ.* **2015**, *106*, 467–476.
- (89) Chen, Z.; Gao, Y.; Xia, F.; Bi, C.; Mo, J. Formation kinetics of SVOC organic films and their impact on child exposure in indoor environments. *Sci. Total Environ.* **2024**, *912*, 168970.
- (90) Liu, Q.-T.; Chen, R.; McCarry, B. E.; Diamond, M. L.; Bahavar, B. Characterization of polar organic compounds in the organic film on indoor and outdoor glass windows. *Environ. Sci. Technol.* **2003**, *37*, 2340–2349.
- (91) Huo, C.-Y.; Liu, L.-Y.; Zhang, Z.-F.; Ma, W.-L.; Song, W.-W.; Li, H.-L.; Li, W.-L.; Kannan, K.; Wu, Y.-K.; Han, Y.-M.; Peng, Z.-X.; Li, Y.-F. Phthalate esters in indoor window films in a northeastern Chinese urban center: film growth and implications for human exposure. *Environ. Sci. Technol.* **2016**, *50*, 7743–7751.
- (92) Wang, L.; Zhao, A.; Wang, K.; Liu, F. Phthalates in glass window films in university dormitories in Beijing, China, and exposure implications. *Build. Environ.* **2021**, *196*, 107813.
- (93) Wallace, L. A.; Ott, W. R.; Weschler, C. J.; Lai, A. C. K. Desorption of SVOCs from heated surfaces in the form of ultrafine particles. *Environ. Sci. Technol.* **2017**, *51*, 1140–1146.
- (94) Weschler, C. J.; Nazaroff, W. W. Growth of organic films on indoor surfaces. *Indoor air* **2017**, *27*, 1101–1112.
- (95) Butte, W.; Heinzow, B. Pollutants in house dust as indicators of indoor contamination. *Rev. Environ. Contam. Toxicol.* **2002**, *175*, 1–46.
- (96) Salthammer, T.; Zhang, Y.; Mo, J.; Koch, H. M.; Weschler, C. J. Assessing human exposure to organic pollutants in the indoor environment. *Angew. Chem., Int. Ed.* **2018**, *57*, 12228–12263.
- (97) Lang, B. E. Solubility of water in octan-1-ol from (275 to 369) K. *J. Chem. Eng. Data* **2012**, *57*, 2221–2226.
- (98) Balasuryia, D.; Queral-Beltran, A.; Vick, T.; Simpson, S.; Lacorte, S.; Aga, D. S.; Hoepker, A. C. Experimental determination of pK_a for 10 PFAS, mono-, di-, and trifluoroacetic acid by ^{19}F -NMR. *Environ. Sci. Technol. Lett.* **2025**, *12*, 1238–1246.
- (99) World Health Organization. *WHO global air quality guidelines. Particulate matter (PM_{2.5} and PM₁₀), ozone, nitrogen dioxide, sulfur dioxide and carbon monoxide*; World Health Organization, Geneva, 2021.
- (100) Yoshida, T.; Mimura, M.; Sakon, N. Intakes of phthalates by Japanese children and the contribution of indoor air quality in their residences. *Environ. Sci. Pollut. Res.* **2020**, *27*, 19577–19591.
- (101) Wang, X.; Tao, W.; Xu, Y.; Feng, J.; Wang, F. Indoor phthalate concentration and exposure in residential and office buildings in Xi'an, China. *Atmos. Environ.* **2014**, *87*, 146–152.
- (102) Huang, L.; Qiao, Y.; Deng, S.; Zhou, M.; Zhao, W.; Yue, Y. Airborne phthalates in indoor environment: partition state and influential built environmental conditions. *Chemosphere* **2020**, *254*, 126782.
- (103) Rudel, R. A.; Camann, D. E.; Spengler, J. D.; Korn, L. R.; Brody, J. G. Phthalates, alkylphenols, pesticides, polybrominated diphenyl ethers, and other endocrine-disrupting compounds in indoor air and dust. *Environ. Sci. Technol.* **2003**, *37*, 4543–4553.
- (104) Rudel, R. A.; Dodson, R. E.; Perovich, L. J.; Morello-Frosch, R.; Camann, D. E.; Zuniga, M. M.; Yau, A. Y.; Just, A. C.; Brody, J. G. Semivolatile endocrine-disrupting compounds in paired indoor and outdoor air in two northern California communities. *Environ. Sci. Technol.* **2010**, *44*, 6583–6590.
- (105) Quintana-Belmares, R. O.; Kraus, A. M.; Esfahani, B. K.; Rosas-Pérez, I.; Mucs, D.; López-Marure, R.; Bergman, Å.; Alfaro-Moreno, E. Phthalate esters on urban airborne particles: levels in PM₁₀ and PM_{2.5} from Mexico City and theoretical assessment of lung exposure. *Environ. Res.* **2018**, *161*, 439–445.
- (106) Yoo, H.; Park, P.; Le, Y. T.-H.; Park, S.; Jung, Y.-W.; Youn, J.-S.; Kim, Y.-M.; Jeon, K.-J. Characterization of tire and road wear microplastics and phthalates in inhalable PM₁₀ road dust: implications for urban air pollution. *Environ. Pollut.* **2025**, *384*, 126991.
- (107) Salthammer, T.; Morrison, G. C. Temperature and indoor environments. *Indoor air* **2022**, *32*, e13022.
- (108) Salthammer, T. The reliability of models for converting formaldehyde emissions from wood-based materials to different environmental conditions. *Build. Environ.* **2024**, *247*, 111041.
- (109) Atkinson, R.; Arey, J. Atmospheric degradation of volatile organic compounds. *Chem. Rev.* **2003**, *103*, 4605–4638.
- (110) Jonsson, Å. M.; Hallquist, M.; Ljungström, E. Impact of humidity on the ozone initiated oxidation of limonene, Δ³-carene, and α-pinene. *Environ. Sci. Technol.* **2006**, *40*, 188–194.
- (111) Clausen, P. A.; Xu, Y.; Kofoed-Sørensen, V.; Little, J. C.; Wolkoff, P. The influence of humidity on the emission of di-(2-ethylhexyl) phthalate (DEHP) from vinyl flooring in the emission cell “FLEC”. *Atmos. Environ.* **2007**, *41*, 3217–3224.
- (112) Liang, Y.; Xu, Y. Emission of phthalates and phthalate alternatives from vinyl flooring and crib mattress covers: The influence of temperature. *Environ. Sci. Technol.* **2014**, *48*, 14228–14237.
- (113) Xiong, J.; Wei, W.; Huang, S.; Zhang, Y. Association between the emission rate and temperature for chemical pollutants in building materials: general correlation and understanding. *Environ. Sci. Technol.* **2013**, *47*, 8540–8547.
- (114) Fan, L.; Wang, L.; Wang, K.; Liu, F. Phthalates in glass window films are associated with dormitory characteristics, occupancy activities and habits, and environmental factors. *Environ. Sci. Pollut. Res.* **2023**, *30*, 32550–32559.